$YBa_2Cu_3O_7$: A nearly antiferromagnetic Fermi liquid

P. Monthoux and D. Pines
Department of Physics, University of Illinois at Urbana-Champaign, 1110 West Green Street, Urbana, Illinois 61801
(Received 25 August 1992)

We have carried out strong-coupling calculations using the Eliashberg formalism, which provide strong evidence for the description of the planar quasiparticles in $YBa_2Cu_3O_7$ as a nearly antiferromagnetic Fermi liquid. We show that when one takes into account the full structure (in frequency and momentum space) of the spin-fluctuation-induced interaction between quasiparticles, a superconducting transition temperature of 90 K is obtained with a dimensionless coupling constant, $\lambda=0.402N(0)g=0.83$, for a hole concentration of 0.25, a quasiparticle spectrum characterized by nearest-neighbor hopping, $t=0.25$ eV, and a spin-fluctuation spectrum determined by experiment. With a next-nearest-neighbor hopping, $t'=-0.45t$, the coupling required to obtain a T_c of 90 K is reduced by some 10%. Strong-coupling calculations of the normal state, using these latter parameters, yield a resistivity that varies linearly with temperature, with a magnitude at 90 K of 62 $\mu\Omega$ cm, a frequency dependence of the optical conductivity in quantitative agreement with experiment for energies ≤ 0.1 eV, a quasiparticle spectrum characterized by a momentum-dependent wave-function renormalization constant, $0.4 \leq Z_p \leq 0.6$, and a self-energy whose imaginary part is proportional to ω for energies up to 0.25 eV. We give a progress report on the extent to which a self-consistent description of the spin-fluctuation excitation spectrum can be found by taking $\chi(\mathbf{q},\omega)=\tilde{\chi}(\mathbf{q},\omega)/[1-J(\mathbf{q})\tilde{\chi}(\mathbf{q},\omega)]$, where $\tilde{\chi}(\mathbf{q},\omega)$ is the irreducible particle-hole susceptibility calculated for quasiparticles coupled to spin excitations whose spectrum is given by $\chi(\mathbf{q},\omega)$ and $J(\mathbf{q})$ is the effective spin-spin coupling.

I. INTRODUCTION

Since the discovery of high-temperature superconductivity in the copper oxides by Bednorz and Mueller,[1] a key question has been "what is the origin of the superconductivity in these systems?" The possibility of d-wave pairing in the context of the Hubbard model was considered by Bickers and co-workers.[2] In three previous paper[3-5] [hereafter referred to as Monthoux, Balatsky, and Pines (MBP) (the first two) and Monthoux and Pines (MP), respectively] we have examined the possibility that spin fluctuations might be a candidate mechanism for high-temperature superconductivity. A similar examination, using somewhat different parameters, has been carried out by Ueda, Moriya, and Takahashi.[6] We have described the results of weak-coupling calculations, which demonstrate that the retarded interaction between planar quasiparticles induced by the exchange of antiferromagnetic paramagnons, whose excitation spectrum was determined by fits to normal-state experiments, leads uniquely to a transition to a superconducting state with $d_{x^2-y^2}$ symmetry.[3,4] However, weak-coupling estimates of the transition temperatures attainable with this model turned out to be unreliable and the "proof of concept" for spin-fluctuation-induced superconductivity only came later from a careful strong-coupling calculation.[5] Theorists had been generally skeptical that spin fluctuations could be effective enough to yield high-temperature superconductivity, primarily because they believed that the short lifetime for the scattering of quasiparticles against spin fluctuations would prevent the quasiparticles from taking sufficient advantage of the spin-fluctuation-induced interaction to superconduct at high temperature. These beliefs were supported by many calculations[7,8] that, however, employed approximations developed in the context of phonon-induced superconductivity and were shown by MP to give poor results when applied to the spin excitation spectrum proposed by Millis, Monien, and Pines[9] (hereafter referred to as MMP). A notable exception was the work of Bickers, and co-workers,[2] in which the full frequency and momentum dependence of the interaction was taken into account for a two-dimensional (2D) Hubbard model. This calculation, which yielded a transition temperature of order 30 K, as well as that of Ref. 5, demonstrates that it is only when the Eliashberg equations are solved allowing for the full momentum dependence of the effective interaction that high transition temperatures are obtained.

Still, many questions remain. Due to strong-coupling effects the transition temperatures are reduced considerably from their weak-coupling values and the high T_c's obtained by MP require relatively large values of the coupling constant g. It is thus necessary to calculate the normal-state properties of the model with such values of g, and we present the results of such calculations here. We also explore the dependence of the calculation of T_c and normal-state properties on the choice of the bare quasiparticle spectra and present our results for the dressed quasiparticle properties in the normal state.

The plan of our paper is the following. In Sec. II we present a comparison of the transition temperatures obtained with different Fermi surfaces for a given value of the doping. We consider the simple nearest-neighbor hopping tight-binding band with hopping parameter $t=0.25$ eV and the inclusion of a next-nearest-neighbor

hopping $t'=-0.45t$. We also give the functional dependence of T_c on the coupling constant in the strong-coupling limit for the case $t'=0$, and discuss the effect of Van Hove singularities on the transition temperature. In Sec. III we discuss the properties of the self-energy, the tunneling density of states and the frequency dependence of the gap at T_c with the coupling constant and chemical potential that yield a T_c of 90 K and an electron density $n=0.75$. In Sec. IV we present our results for the temperature dependence of the electrical resistivity, the frequency and temperature dependence of the optical conductivity with the parameters required to obtain a strong-coupling transition temperature of 90 K, for both Fermi surfaces, $t'=0$ and $t'=-0.45t$. In Sec. V, we give a progress report on the extent to which a self-consistent description of the spin-fluctuation excitation spectrum can be found by taking $\chi(\mathbf{q},\omega)=\tilde{\chi}(\mathbf{q},\omega)/[1-J(\mathbf{q})\tilde{\chi}(\mathbf{q},\omega)]$, where $\tilde{\chi}(\mathbf{q},\omega)$ is the irreducible particle-hole susceptibility calculated for quasiparticles coupled to spin excitations whose spectrum is given by $\chi(\mathbf{q},\omega)$ and $J(\mathbf{q})$ is the effective spin-spin coupling; as a first step toward self-consistency, we show that for a suitable choice of $J(\mathbf{q})$, the $\chi(\mathbf{q},\omega)$ that one obtains with the irreducible particle-hole $\tilde{\chi}(\mathbf{q},\omega)$ calculated for quasiparticles coupled to the MMP spin excitation spectrum is close to the input susceptibility $\chi_{\mathrm{MMP}}(\mathbf{q},\omega)$. Section VI contains our conclusions.

II. THE SUPERCONDUCTING TRANSITION TEMPERATURE

Following MBP, the simple model Hamiltonian for the planar quasiparticles is given by

$$\mathcal{H}=\mathcal{H}_0+\mathcal{H}_{\mathrm{int}} , \tag{1a}$$

where

$$\mathcal{H}_0=\sum_{\mathrm{p},\sigma}\epsilon_{\mathrm{p}}\psi^{\dagger}_{\mathrm{p},\sigma}\psi_{\mathrm{p},\sigma} \tag{1b}$$

describes the quasiparticle excitations of energy ϵ_{p}. We will consider two bare quasiparticle spectra ϵ_{p}. The first and simplest is the nearest-neighbor tight-binding dispersion relation

$$\epsilon_{\mathrm{p}}=-2t[\cos(p_x a)+\cos(p_y a)] , \tag{1c}$$

with $t=0.25$ eV. a is the lattice constant. This spectrum has the perfect nesting property at half-filling with the Van Hove singularity at E_F. Upon hole doping, the wave vectors that span the Fermi surface are then smaller than $|\mathbf{Q}|$ where $\mathbf{Q}=(\pi/a,\pi/a)$ and the Van Hove singularity is above the Fermi level. However, photoemission experiments[10] suggest that this spectrum is not realistic for $YBa_2Cu_3O_7$ and that a more appropriate dispersion relation includes a next-nearest-neighbor hopping

$$\epsilon_{\mathrm{p}}=-2t[\cos(p_x a)+\cos(p_y a)]-4t'\cos(p_x a)\cos(p_y a) , \tag{1d}$$

with $t'=-0.45t$. The bandwidth is still $8t=2$ eV. With this next-nearest-neighbor hopping the Fermi surface is never perfectly nested, the Van Hove singularity is at the Fermi level for an electron doping below one half and with an electron density $n=0.75$, the Van Hove singularity is below the Fermi level. Another important feature of this dispersion relation is that in contrast to the nearest-neighbor tight-binding form, Eq. (1c), there are pieces of the Fermi surface that are connected by the antiferromagnetic wave vector $\mathbf{Q}$ below half filling.

$\mathcal{H}_{\mathrm{int}}$ describes an effective spin-spin interaction between the planar quasiparticles, which we model phenomenologically as an interaction between the planar quasiparticle excitations and the spin fluctuations. We thus write it as

$$\mathcal{H}_{\mathrm{int}}=\frac{1}{\Omega}\sum_{\mathbf{q}}\bar{g}(\mathbf{q})\mathbf{s}(\mathbf{q})\cdot\mathbf{S}(-\mathbf{q}) , \tag{1e}$$

where

$$\mathbf{s}(\mathbf{q})=\frac{1}{2}\sum_{\alpha,\beta,\mathbf{k}}\psi^{\dagger}_{\mathbf{k}+\mathbf{q},\alpha}\boldsymbol{\sigma}_{\alpha\beta}\psi_{\mathbf{k},\beta} , \tag{1f}$$

and $\mathbf{S}$ is the spin-fluctuation operator whose properties are determined by the spin-spin correlation function $\chi_{ij}(\mathbf{q},\omega)=\delta_{ij}\chi(\mathbf{q},\omega)$. The interaction has to be short ranged and thus $\bar{g}(\mathbf{q})$ should not be very momentum dependent. For simplicity we will ignore the momentum dependence of the coupling to spin fluctuations and set $\bar{g}(\mathbf{q})=\bar{g}$. Moreover, we require that $\chi(\mathbf{q},\omega)$ be such as to provide a quantitative fit to NMR experiments. We choose to use the low-frequency form of $\chi(\mathbf{q},\omega)$ determined by NMR, because as yet neutron-scattering experiments have not produced a consensus on the behavior of $\chi(\mathbf{q},\omega)$ in the frequency range 1–50 meV. We thus adopt the form of $\chi(\mathbf{q},\omega)$ proposed by Millis, Monien, and Pines, which has been shown to provide a quantitative fit to the NMR experiments involving ^{63}Cu, ^{17}O, and ^{89}Y, in the $YBa_2Cu_3O_7$ superconductor:

$$\chi_{\mathrm{MMP}}(\mathbf{q},\omega)=\frac{\chi_{\mathbf{Q}}}{1+\xi^2(\mathbf{q}-\mathbf{Q})^2-i\omega/\omega_{\mathrm{SF}}} , \quad q_x>0 , \quad q_y>0 , \tag{2}$$

where $\chi_{\mathbf{Q}}$ is the static spin susceptibility at wave vector $\mathbf{Q}=(\pi/a,\pi/a)$. In the normal state, $\chi_{\mathbf{Q}}\equiv\chi_0(\xi/a)^2\beta^{1/2}$, where χ_0 is the experimentally measured long-wavelength spin susceptibility, which is in general temperature dependent, ξ is a temperature-dependent antiferromagnetic correlation length, $\beta\approx\pi^2$. With this form of $\chi(\mathbf{q},\omega)$ there are no well defined low-frequency magnetic excitations, but rather one has a relaxational mode, the paramagnon, whose energy is given by

$$\omega_{\mathrm{SF}}=\frac{\Gamma}{\beta^{1/2}\pi(\xi/a)^2} , \tag{3}$$

where $\Gamma\approx 0.4$ eV plays the role of a magnetic Fermi energy. The fits to NMR experiments on $YBa_2Cu_3O_7$ yield $\xi(T_c)\sim 2.3a$ and hence $\omega_{\mathrm{SF}}(T_c)\sim 8$ meV.

Our phenomenological model Hamiltonian, specified by Eqs. (1a)–(1f), leads to a self-consistent description of the spin behavior of the system to the extent that the resulting *calculated quasiparticle spin-fluctuation spectral density*, $\chi(\mathbf{q},\omega)$, agrees with the input value, $\chi_{\mathrm{MMP}}(\mathbf{q},\omega)$.

We carry out this comparison in Sec. V.

The 2D Eliashberg equations[11] for the critical temperature of a single CuO plane in the Matsubara representation reduce, in the case of a spin-fluctuation-induced interaction between the quasiparticles, to

$$\Sigma(\mathbf{p},i\omega_n)=g^2\frac{k_BT}{N_{\mathbf{q}}^2}\sum_{\Omega_n}\sum_{\mathbf{q}}\chi(\mathbf{p}-\mathbf{q},i\omega_n-i\Omega_n)G(\mathbf{q},i\Omega_n)\ , \tag{4}$$

$$G(\mathbf{p},i\omega_n)=\frac{1}{i\omega_n-(\epsilon_{\mathbf{p}}-\mu)-\Sigma(\mathbf{p},i\omega_n)}\ , \tag{5}$$

$$\Phi(\mathbf{p},i\omega_n)=-g^2\frac{k_BT}{N_{\mathbf{q}}^2}\sum_{\Omega_n}\sum_{\mathbf{q}}\chi(\mathbf{p}-\mathbf{q},i\omega_n-i\Omega_n)G(\mathbf{q},i\Omega_n)\times G(-\mathbf{q},-i\Omega_n)\Phi(\mathbf{q},i\Omega_n)\ , \tag{6}$$

where $\Sigma(\mathbf{p},i\omega_n)$ is the self-energy, $G(\mathbf{p},i\omega_n)$ is the one-particle Green's function, $\Phi(\mathbf{p},i\omega_n)$ is the anomalous self-energy and is proportional to the order parameter, $\epsilon_{\mathbf{p}}$ is the bare electron spectrum, and μ is the chemical potential. $N_{\mathbf{q}}^2$ is the total number of momenta in the Brillouin zone and $\omega_n=(2n+1)\pi k_BT$, $n=-\infty,\ldots,-1,0,1,\ldots,+\infty$. For convenience, the coupling constant g^2 is chosen to be equal to $2g_{\text{eff}}^2$ as defined in MBP, that is $g^2=3/4\bar{g}^2$. $\chi(\mathbf{q},i\nu_n)$ is related to the imaginary part of the spin response function $\text{Im}\chi(\mathbf{q},\omega)$, Eq. (2), via the spectral representation

$$\chi(\mathbf{q},i\nu_n)=-\int_{-\infty}^{+\infty}\frac{d\omega}{\pi}\frac{\text{Im}\chi(\mathbf{q},\omega)}{i\nu_n-\omega}\ . \tag{7}$$

To get $\chi(\mathbf{q},i\nu_n)$ to decay faster than $1/\nu_n$ for large ν_n, we introduce a cutoff ω_0 and take $\text{Im}\chi(\mathbf{q},\omega)=0$ for $\omega>\omega_0$. In the following we will adopt the value $\omega_0=0.4$ eV.

The equations are solved with a fast Fourier transform (FFT) algorithm on a 64×64 lattice, with a Matsubara frequency cutoff of $\sim$three times the bandwidth, that is ~6 eV.[5] Because the bandwidth of the tight-binding dispersion relation with next-nearest-neighbor hopping is independent of t', it is possible to use the same number of Matsubara frequencies with both bare quasiparticle spectra for a fixed ratio $\max(|\omega_n|)$ to the bandwidth (one must keept this ratio fixed in order not to introduce fictitious temperature dependences). This is very important, since the FFT algorithm requires one to use a number of Matsubara frequencies that can be expressed as a product of powers of 2, 3, and 5, that is a limited number of temperatures. It is only because the bandwidths of the two dispersion relations Eqs. (1c) and (1d) are equal no matter what t' is that one is able to calculate all properties at the same temperatures for both cases, which is a great advantage.

The critical temperature for the model is determined from Eq. (6), which is an eigenvalue equation for the vector $\Phi(\mathbf{p},i\omega_n)$. A nonzero solution for the order parameter can be found when the largest eigenvalue of the matrix

$$\mathcal{K}(\mathbf{p},i\omega_n;\mathbf{q},i\Omega_n)=-g^2(k_BT/N_{\mathbf{q}}^2)\chi(\mathbf{p}-\mathbf{q},i\omega_n-i\Omega_n)\times G(\mathbf{q},i\Omega_n)G(-\mathbf{q},i\Omega_n)$$

is equal to one. For the present model the argument presented for the weak-coupling case still holds: A nontrivial solution can only be found for a d-wave gap

$$\Phi(\mathbf{p},i\omega_n)\propto\cos(p_xa)-\cos(p_ya)\ .$$

Figure 1 shows the relation $T_c=T_c(g)$ for the bare quasiparticle dispersion relation Eq. (1c) along with the MBP weak-coupling calculation, and the strong-coupling result one obtains upon making the approximations proposed by Millis[12] and that have been used by other authors.[8] The difference is physically significant, and one does not reach the conclusion that spin fluctuations can yield high transition temperatures unless one solves the full problem, i.e., with the complete momentum dependence of the effective interaction.

It is interesting to note in the case $t'=0$, for coupling constants greater or equal to the coupling constant, $g=1.53$ eV, required to obtain $T_c=90$ K, the transition temperature may be written as

$$T_c=0.636\frac{\Gamma}{\pi^2}\exp\left[-\frac{1}{0.402N(0)g}\right]\ , \tag{8}$$

where $N(0)=-(2/\pi N_{\mathbf{p}}^2)\sum_{\mathbf{p}}\text{Im}G_R(\mathbf{p},0)$ is the tunneling density of states for both spin orientations calculated from the "no lines crossing" one-particle Green's function at T_c. $N(0)$ is obtained by analytic continuation using N-point Padé approximants.[13] The above formula gives T_c to an accuracy of at least 0.2% for the four data points that we considered ($T_c=90$, 96, 100, and 108 K). For $T_c=90$ K, one has $g^2=2.35$ eV^2, $N(0)_{g^2,T_c}=1.349$ states/eV. The values for $T_c=96$ K are $g^2=2.85$ eV^2, $N(0)_{g^2,T_c}=1.301$ states/eV, and for $T_c=100$ K one has

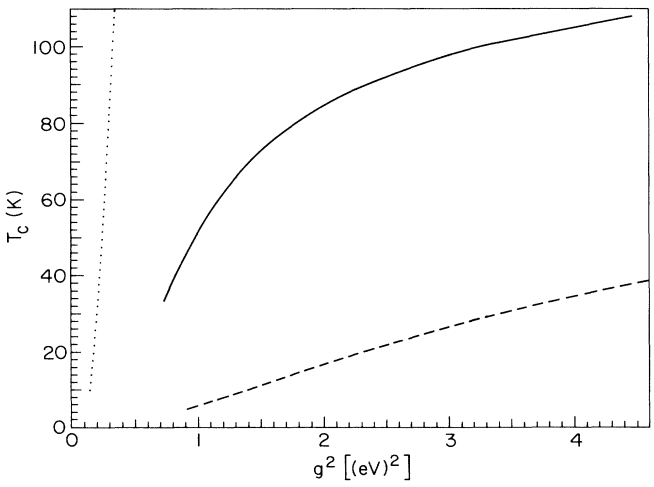

FIG. 1. The critical temperature T_c vs coupling constant squared. The full line is the result of the strong-coupling calculation, the dotted line is the weak-coupling result obtained by MBP, while the dashed line is the result obtained using the "phonon-inspired" Eliashberg calculation of Millis (Ref. 12), all calculated for the same model parameters.

$g^2=3.28$ eV^2, $N(0)_{g^2,T_c}=1.257$ states/eV. Finally, for $T_c=108$ K the numbers are $g^2=4.50$ eV^2, $N(0)_{g^2,T_c}=1.151$ states/eV. Another quantity of interest is the value of the expression in the exponential in Eq. (8). At $T_c=90$ K one has $0.402N(0)g=0.83$.

We see that the strong-coupling expression for the critical temperature takes a form similar to the weak-coupling expression obtained by MBP, except that the dimensionless coupling constant $\lambda_w \sim N^2(0)g^2$ is replaced by const$\times\sqrt{\lambda_w}$ (where const is a numerical factor of order unity). A similar coupling-constant dependence was previously found by Hirsch and Scalapino[15] in perturbation-theoretic and Monte Carlo calculations that examined the role which Van Hove singularities in low-dimensional systems play in enhancing T_c. In the present case, with an electron density of $n=0.75$, the Fermi surface is far from the Van Hove singularity; it is conceivable that the strong-coupling aspects of our calculation make it possible for Van Hove singularities to make a significant contribution to the pairing interaction despite their comparatively large distance from the Fermi surface. It is interesting to note that the prefactor in Eq. (8) is smaller than the weak-coupling result by about a factor of two. Since the quasiparticle damping becomes large much more rapidly than in usual Fermi liquids as one moves away from the Fermi surface, the range of frequencies that can contribute to the pairing is reduced compared to its weak-coupling value.

The coupling constant that yields a $T_c=90$ K superconductor is $g^2=2.35$ eV^2 when using the nearest-neighbor tight-binding dispersion relation. The chemical potential of the interacting system is then about 140 meV lower than that of the noninteracting electron gas with the same density. If one uses the more realistic spectrum that includes next-nearest-neighbor hopping with $t'=-0.45t$, the coupling constant required to get a transition temperature of 90 K is smaller, namely $g^2=1.85$ eV^2. Interestingly, the chemical potential in this case is hardly changed (only a few meV) from that of the free-electron gas of the same density. There are several differences between the two dispersion relations, Eqs. (1c) and (1d). We have already mentioned that the spectrum with next-nearest-neighbor hopping has the property that pieces of the Fermi surface are spanned by the antiferromagnetic wave vector **Q**. That implies that one is better able to take advantage of the spin-fluctuation-mediated interaction, which is sharply peaked at **Q**. However, the self-energy is also sensitive to the better match between the wave vectors spanning the Fermi surface and **Q**, and is likely to be larger as well. To the extent that these two effects cancel each other out, the smaller coupling constant required to obtain a transition temperature of 90 K can be attributed to the larger density of states at the Fermi level that one obtains with the spectrum Eq. (1d) [see next section and Figs. 5(a) and 5(b)].

III. QUASIPARTICLE PROPERTIES AND GAP STRUCTURE

Self-energy corrections arising from the coupling of quasiparticles to spin fluctuations have been calculated previously by Kampf and Schrieffer,[14] who determined first-order corrections to the self-energy at $T=0$ for a wide range of values of the correlation length ξ/a, and by Bickers and White,[2] who for specific choice of Hubbard model parameters, calculated quasiparticle properties in a conserving approximation and examined as well its parquet extension. In the present context, to obtain dynamical information on our model, one needs to look at the self-energy on the real frequency axis. This is accomplished by analytic continuation of $\Sigma(\mathbf{p},i\omega_n)$ using N-point Padé approximants.[13] Figure 2 shows the frequency dependence of imaginary part of the self-energy with $t'=-0.45t$ at $T=90$ K for two points on the Fermi surface, and the real part is displayed in Fig. 3. Our first-order perturbation-theoretic results are similar to those found by Kampf and Schrieffer[14] for comparable values of ξ/a. The coupling constant was chosen to yield a T_c of 90 K. $\mathrm{Im}\Sigma(\mathbf{p}_F,\omega)$ goes like $\alpha T+\gamma\omega^2$, for frequencies

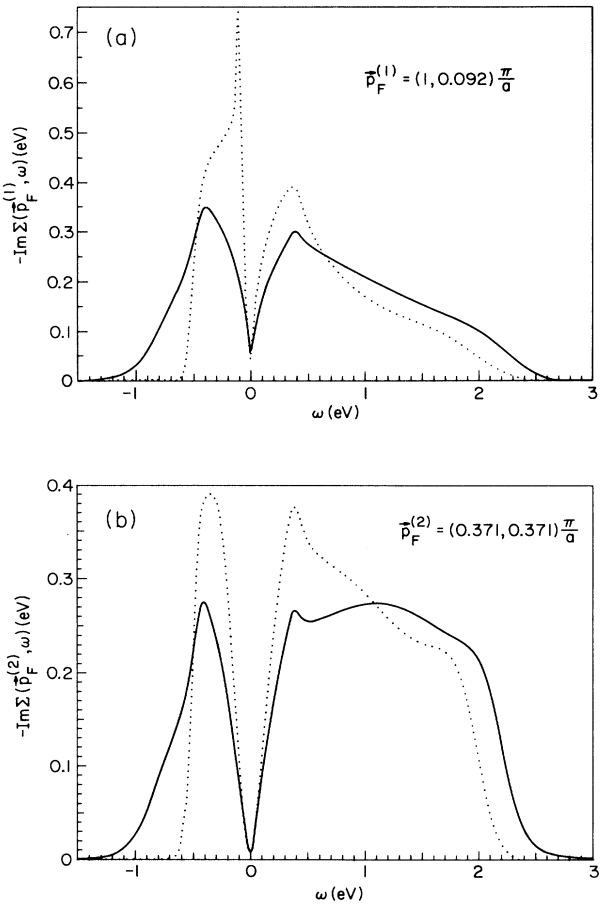

FIG. 2. The frequency dependence of the imaginary part of the self-energy for $t'=-0.45t$ at $T=90$ K for two representative momenta on the Fermi surface and with the coupling constant required to obtain a transition temperature of 90 K. The full line is the self-consistent result in the no lines crossing approximation, and the dotted line shows the first-order perturbation theoretic result for the same parameters. (a) shows $-\mathrm{Im}\Sigma(\mathbf{p},\omega)$ vs ω for $\mathbf{p}=\mathbf{p}_F^{(1)}\equiv(1,0.092)\pi/a$ and (b) shows $-\mathrm{Im}\Sigma(\mathbf{p},\omega)$ vs ω for $\mathbf{p}=\mathbf{p}_F^{(2)}\equiv(0.371,0.371)\pi/a$.

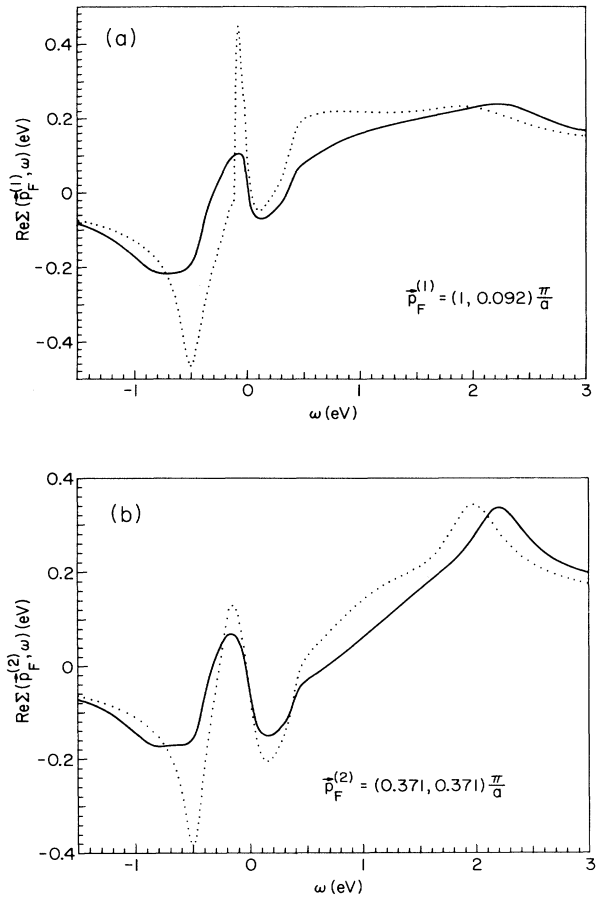

FIG. 3. The frequency dependence of the real part of the self-energy for the same parameters as in Fig. 2. The full line is the self-consistent result in the no lines crossing approximation, and the dotted line shows the first-order perturbation theoretic result for the same coupling constant and chemical potential. (a) shows $\mathrm{Re}\Sigma(\mathbf{p},\omega)$ vs ω for $\mathbf{p}=\mathbf{p}_F^{(1)}\equiv(1,0.092)\pi/a$ and (b) shows $\mathrm{Re}\Sigma(\mathbf{p},\omega)$ vs ω for $\mathbf{p}=\mathbf{p}_F^{(2)}\equiv(0.371,0.371)\pi/a$. The sharp feature in the real part of the first-order perturbation theoretic $\mathrm{Re}\Sigma(\mathbf{p},\omega)$ at $\omega\approx-0.5$ eV is associated with the rapid drop of the imaginary part of the self-energy at the same frequency seen in Fig. 2. A similar feature is present at $\omega\approx2$ eV but not as pronounced because the density of states near the top of the band is smaller.

smaller than the characteristic spin-fluctuation frequency ω_{SF}, where α and γ are constants. However, the imaginary part of the self-energy becomes linear in ω for frequencies large compared to ω_{SF}. It is interesting to note that near the Van Hove singularity, at $\mathbf{p}_F^{(1)}\equiv(1,0.092)\pi/a$, the crossover from quadratic to linear ω behavior occurs at lower values of ω.

As may be seen in Fig. 3, $\mathrm{Re}\Sigma(\mathbf{p}_F,0)\neq0$ and thus the chemical potential is changed by the interactions. Because of the momentum dependence of the real part of the self-energy at $\omega=0$ that reflects both the influence of the scattering against spin fluctuations and the tight-binding spectrum with next-nearest-neighbor hopping $t'=-0.45t$, the shape of the Fermi surface is slightly changed by the interactions but its area remains constant. Figure 4 shows that the point $\mathbf{p}_F^{(1)}$ on the interacting Fermi surface is closer to the Van Hove singularity than the corresponding point on the Fermi surface obtained from the bare quasiparticle spectrum Eq. (1d) with $t'=-0.45t$. Also shown in Figs. 2 and 3 are the results one obtains with the bare Green's function in Eq. (4) for the self-energy. The difference between the first-order perturbation-theoretic result and the self-consistent one is most important at $\mathbf{p}_F^{(1)}$, the point on the Fermi surface closest to the Van Hove singularity. For instance, at $\mathbf{p}_F^{(1)}$ the quasiparticle residue

$$Z_{\mathbf{p}_F^{(1)}}=\left[1-\frac{\partial\,\mathrm{Re}\Sigma(\mathbf{p}_F^{(1)},\omega)}{\partial\omega}\right]^{-1}\Bigg|_{\omega=0}$$

one obtains in first order is 0.212, whereas the self-consistent result is 0.407, nearly a factor of two larger. On the other hand, at $\mathbf{p}_F^{(2)}$, the first-order result for $Z_{\mathbf{p},F}^{(2)}$ is 0.495 and the self-consistent one 0.560, which is about a 12% difference. Therefore, we conclude that self-consistency is especially important for the points on the Fermi surface that are near Van Hove singularities. The difference between the first-order quasiparticle residue and the self-consistent result is very important in our case, since the $d_{x^2-y^2}$ gap on the Fermi surface is maximum at $\mathbf{p}_F^{(1)}$. A first-order perturbation-theoretic calculation of lifetime effects on T_c would overestimate the importance of self-energy corrections. We also have calculated the quasiparticle residue in the case $t'=0$, to check the effect of the Fermi surface shape on that quantity. The representative points on the Fermi surface are now $\mathbf{p}_F^{(1)}\equiv(0.781,0)\pi/a$ and $\mathbf{p}_F^{(2)}\equiv(0.449,0.449)\pi/a$. In this case one has $Z_{\mathbf{p}_F^{(1)}}=0.410$ and $Z_{\mathbf{p}_F^{(2)}}=0.471$. The quasi-

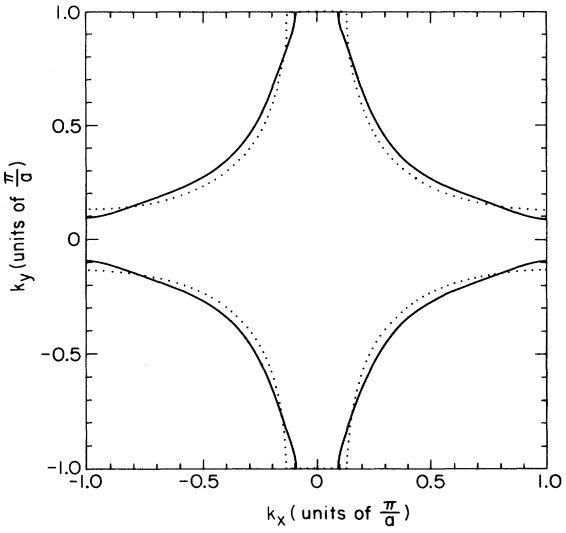

FIG. 4. The Fermi surface with $t'=-0.45t$ and 0.25 hole doping. The full line is the Fermi surface obtained with self-energy corrections, $\epsilon_{\mathbf{p}}-\mu+\mathrm{Re}\Sigma(\mathbf{p},0)=0$, and the dotted line is the Fermi surface for the noninteracting system $\epsilon_{\mathbf{p}}-\mu_0=0$, where μ_0 is the chemical potential that gives $n=0.75$ when $\mathrm{Re}\Sigma(\mathbf{p},0)=0$.

particle residue is larger along the diagonal in both cases and the Fermi surface shape does not have a large influence on its magnitude.

The quasiparticle effective mass on the Fermi surface m_x^* along the x axis is given by

$$\frac{m_x^*}{m_x}=Z_{\mathbf{p}_F}^{-1}\Big/\left[1+\frac{m_x}{p_{F_x}}\frac{\partial\,\mathrm{Re}\Sigma(\mathbf{p},0)}{\partial p_x}\bigg|_{\mathbf{p}=\mathbf{p}_F}\right], \tag{9}$$

where m_x is defined via $\partial\epsilon_{\mathbf{p}}/\partial p_x|_{\mathbf{p}=\mathbf{p}_F}\equiv p_{F_x}/m_x$. There are thus two contributions to the effective mass, one coming from the frequency dependence of the self-energy and the other from its momentum dependence. It was found by one of us[16] in a first-order perturbation-theoretic calculation (with much smaller coupling constants than those reported here) that the momentum dependence of the self-energy only contributed about 10% to the effective mass. A similar result is to be expected here and can be understood by the following argument. The denominator in Eq. (9) can be written as $1+[\partial\,\mathrm{Re}\Sigma(\mathbf{p},0)/\partial p_x](\partial\epsilon_{\mathbf{p}}/\partial p_x)^{-1}$. The real part of the self-energy $\mathrm{Re}\Sigma(\mathbf{p},0)$ and $\epsilon_{\mathbf{p}}$ are smooth functions of the momentum $\mathbf{p}$. Thus their derivatives with respect to $\mathbf{p}$ should be, in appropriate units, of the same order of magnitude as the functions themselves. Note that when $\partial\epsilon_p/\partial p_x$ vanishes for symmetry reasons, so does $\partial\mathrm{Re}\Sigma(\mathbf{p},0)/\partial p_x$ and the ratio remains finite. Now, $\epsilon_{\mathbf{p}}$ is of the order of 1 eV and $\mathrm{Re}\Sigma(\mathbf{p},0)$ of the order of 0.1 eV as can be seen from Fig. (3). The denominator in Eq. (9) is thus expected to be about 1.1, and therefore within, say 20%, the mass enhancement is given by the inverse of the quasiparticle residue, namely between 1.8 at $\mathbf{p}_F^{(2)}$ and 2.5 at $\mathbf{p}_F^{(1)}$. To conclude, we note that in spite of the strong coupling, the quasiparticle mass enhancement is only moderate.

The results for $\Sigma(\mathbf{p}_F^{(1)},\omega)$ shown in Figs. 2 and 3 have another interesting feature. One notices that both the real and imaginary parts of $\Sigma(\mathbf{p}_F^{(1)},\omega)$ calculated in first order have a very strong frequency dependence for frequencies slightly below the Fermi level and a very sharp peak. This peak is precisely located at the Van Hove singularity. This feature is totally absent in the self-consistent result; the Van Hove singularity has no direct effect on the frequency dependence of the self-energy calculated in the no lines crossing Eliashberg approximation.

The tunneling density of states $N(\omega)=-(1/\pi N_{\mathbf{p}}^2)\sum_{\mathbf{p}}\mathrm{Im}G_R(\mathbf{p},\omega)$ for one spin orientation, obtained from $G(\mathbf{p},i\omega_n)$ by analytic continuation using N-point Padé approximants,[13] for both $t'=0$ and $t'=-0.45t$ are shown in Figs. 5(a) and 5(b), respectively. The temperature is 90 K and the coupling constant was chosen to yield a T_c of 90 K. Also shown are the densities of states for the noninteracting systems of the same density. It is obvious from the plots that lifetime effects seriously affect the influence of the Van Hove singularity on $N(\omega)$, although in the $t'=0$ case the remnant of the singularity has been shifted to the Fermi level. This may remind the reader of the effect we discussed in Sec. II, where it was argued that because of the strong coupling the functional dependence of T_c on the coupling constant

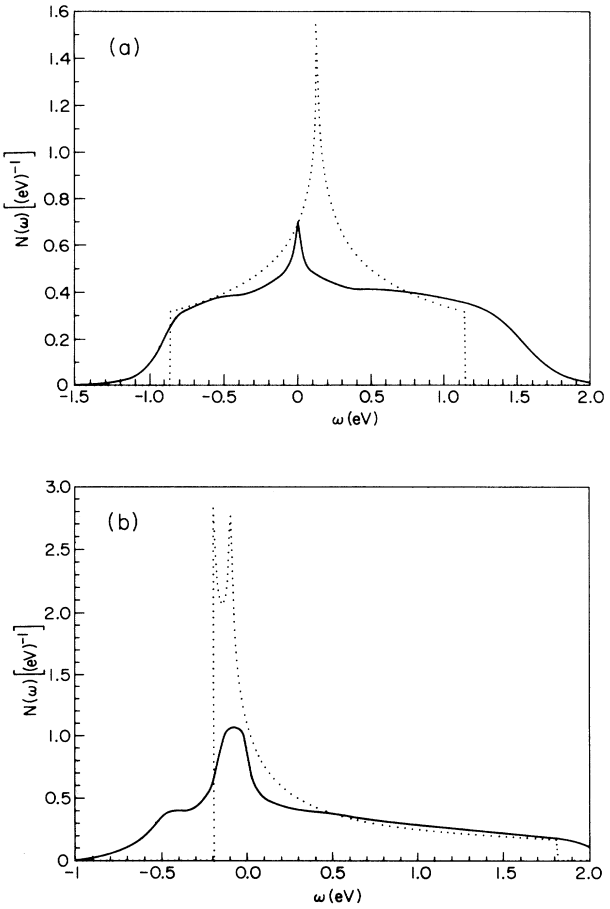

FIG. 5. The frequency-dependent tunneling density of states $N(\omega)=-(1/\pi)\mathrm{Tr}[\mathrm{Im}G_R(\mathbf{p},\omega)]$ for the noninteracting system (dotted line) and with the no lines crossing Eliashberg one-particle Green's function (full line). (a) shows the case $t'=0$; note how the Van Hove singularity, which is far from the Fermi level is broadened by lifetime effects and shited towards $\omega=0$. (b) shows the case $t'=-0.45t$. The large density of states near the bottom of the band is due to the fact that the dispersion relation Eq. (1d) is very flat near $\mathbf{p}=(0,0)$. Note also the much larger particle-hole asymmetry compared to (a), and the considerable reduction of the twin peaks by lifetime effects.

was affected by the Van Hove singularity, in spite of the relative distance of the latter from the Fermi surface. It will be interesting to see if one gets the same effect with the more realistic bare quasiparticle spectrum with next-nearest-neighbor hopping.

On comparing Figs. 5(a) and 5(b), one also sees that the tunneling density of states at the Fermi level is larger for $t'=-0.45t$. The plot of the tunneling density of states actually provides us with an estimate of the contribution of the momentum dependence of the self-energy to the quasiparticle effective mass. For $\omega\approx 0$ we can approximately write $G_R(\mathbf{p},\omega)\approx Z_{\mathbf{p}}/(\omega-E_{\mathbf{p}}+i\delta)$ where $E_{\mathbf{p}}$ is the renormalized quasiparticle spectrum with effective mass m^*. The tunneling density of states at the Fermi level $\{N(0)=-(1/\pi)\mathrm{Tr}[\mathrm{Im}G_R(\mathbf{p},0)]\}$ is thus given by Z times the density of states of a noninteracting system of

quasiparticles of mass m^*. To the extent that the momentum dependence of $\mathrm{Re}\Sigma(\mathbf{p},0)$ does not contribute appreciably to m^*, then $(m^*/m)Z \approx 1$ and the tunneling density of states at E_F is not changed very much by the interactions. Figures 5(a) and 5(b) demonstrate that even though the interactions can change the overall shape of the tunneling density of states $N(\omega)$ substantially, the value of $N(0)$ for the free-electron system and the value of $N(0)$ for the interacting system are not very different [the difference is $\sim 1\%$ when $t'=0$, Fig. 5(a)] and $\sim 20\%$ when $t'=-0.45t$ [Fig. 5(b)]. It is interesting to note that, as we have pointed out, the renormalization of the chemical potential is very small when a next-nearest-neighbor hopping $t'=-0.45t$ is included (a few meV, to be compared with 140 meV when $t'=0$), signaling a very small value of $\mathrm{Re}\Sigma(\mathbf{p},0)$ for $\mathbf{p}$ on the Fermi surface (see Fig. 3). We would therefore expect the contribution to the effective mass from the momentum dependence of the self-energy to be even smaller when $t'=-0.45t$ than was found by one of us[16] in the case of $t'=0$. Figures 5(a) and 5(b) show that this is not the case, since the tunneling density of states $N(0)$ is more changed by the interactions for $t'=-0.45t$ than with $t'=0$. This is an indication that $\mathrm{Re}\Sigma(\mathbf{p},0)$ is more strongly momentum dependent for $\mathbf{p}$ near the Fermi surface when $t'=-0.45t$, than when $t'=0$.

As we have shown, self-consistency in the calculation of the self-energy is important given the relatively large coupling constants required to obtain high transition temperatures and the proximity of Van Hove singularities. In fact, for these coupling constants, a first-order perturbation-theoretic calculation of the self-energy gives results that are not compatible with Luttinger's theorem, in that the doping obtained by integrating the tunneling density of states calculated with the first-order self-energy $\Sigma^{(1)}(\mathbf{p},\omega)$ is not equal to the area enclosed by the Fermi surface, the latter being given by the equation $\epsilon_{\mathbf{p}}-\mu+\mathrm{Re}\Sigma^{(1)}(\mathbf{p},0)=0$.[16] It is only when the self-energy is computed self-consistently that the agreement is restored. We have actually used this fact as a check on the consistency of the analytic continuation using Padé approximants for both the density of states and the self-energy.

The frequency dependence of the gap, obtained by analytic continuation using N-point Padé approximants,[13] at $T_c=90$ K is shown in Figs. 6(a) and (b) for $t'=0$ (in order to compare with the MBP calculation) at the point $\mathbf{p}_F^{(1)}\equiv(0.781,0)\pi/a$ on the Fermi surface where the gap is maximum. The weak-coupling result is the one obtained from Eq. (6) where the no lines crossing Green's functions are replaced by free particle propagators and $\Phi(\mathbf{p},i\omega_n)=\Delta(\mathbf{p},i\omega_n)$; in strong coupling,

$$\Phi(\mathbf{p},i\omega_n)=\Delta(\mathbf{p},i\omega_n)\left[1-\frac{\mathrm{Im}\Sigma(\mathbf{p},i\omega_n)}{\omega_n}\right].$$

This is different from MBP in that the frequency dependence of the gap is taken into account, and thus $\Delta(\mathbf{p},\omega)$ will in general be complex. It is interesting to note that by the time one reaches the MBP cutoff, $\propto\Gamma/\pi^2$, of about 50 meV, the imaginary part of $\Delta(\mathbf{p}_F^{(1)},\omega)$ is as large

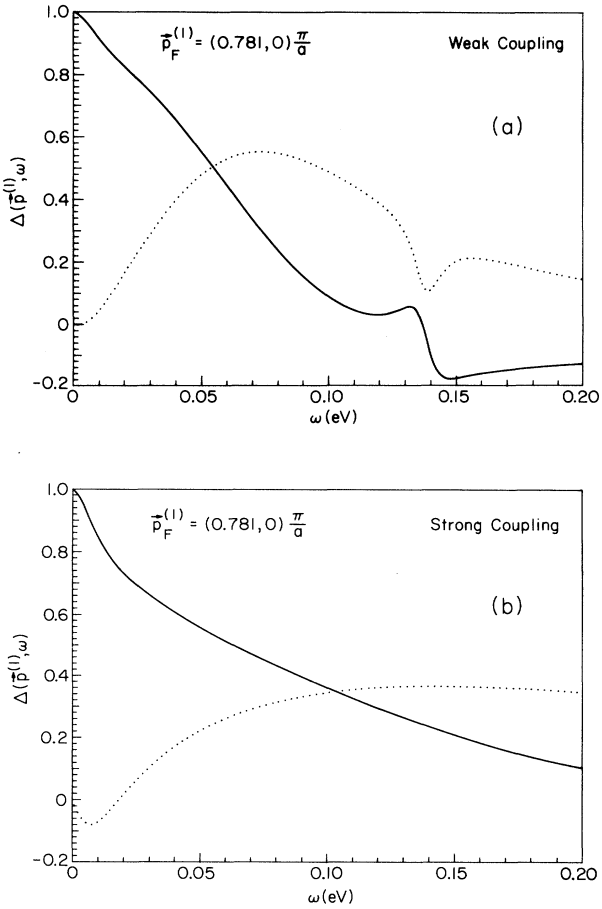

FIG. 6. The frequency dependence of the real (full line) and imaginary part (dashed line) of the gap at $T_c=90$ K for $t'=0$. The point on the Fermi surface is chosen as that where $\Delta(\mathbf{p}_F,\omega)$ is maximum, $\mathbf{p}_F^{(1)}\equiv(0.781,0)\pi/a$. The normalization convention is such that $\mathrm{Re}\Delta(\mathbf{p}_F^{(1)},0)=1$. (a) shows the weak-coupling result obtained from Eq. (6) with $G(\mathbf{q},i\Omega_n)$ replaced by bare propagators. (b) shows the strong-coupling frequency-dependent gap.

as the real part. It is thus not a good approximation to ignore the imaginary part of $\Delta(\mathbf{p},\omega)$ even when self-energy effects are not accounted for. As a consequence of this, part of the large difference between the MBP T_c and the transition temperature one obtains solving the strong-coupling Eliashberg equations (see Fig. 1), is due to the neglect by MBP of the imaginary part and frequency dependence of the gap; the rest is due to self-energy effects. The coupling constant that yields $T_c=90$ K, in a weak-coupling calculation where the frequency dependence of the gap is taken into account, $g^2=0.545$ eV^2, gives a transition temperature of about 225 K when using the MBP gap equation. Still, strong-coupling effects remain the dominant cause for the reduction in T_c, since that coupling constant would yield a strong-coupling transition temperature well below the lowest temperature, $T=33.75$ K, achievable in the present calculation because of computer memory constraints; the coupling constant required to get a strong coupling T_c of 33.75 K

is $g^2=0.75$ eV^2. As was the case with the normal-state self-energy, one notices a feature in the frequency dependence of the weak-coupling gap at about 140 meV. With $t'=0$ and $n=0.75$, this is precisely at the Van Hove singularity. The latter produces a peak in $\mathrm{Im}\Delta(\mathbf{p}_F^{(1)},\omega)$ at $\omega\approx 140$ meV and the corresponding dispersive structure in $\mathrm{Re}\Delta(\mathbf{p}_F^{(1)},\omega)$ at the same frequency. As was the case with the normal-state self-energy, this feature disappears when lifetime effects are taken into account in the one-loop approximation.

IV. OPTICAL CONDUCTIVITY AND RESISTIVITY

Another normal-state property of interest is the frequency-dependent optical conductivity, which, for an applied field in the direction of a CuO plane, is given by

$$\sigma(\omega)=\frac{2e^2}{\hbar c}\bar{\sigma}(\omega)\ , \tag{10a}$$

where c is the lattice constant along the z axis, the factor of 2 comes from the two CuO planes per unit cell, and the dimensionless function $\bar{\sigma}(\omega)$ is expressed in terms of the current-current correlation function $R(\omega)$ as

$$\bar{\sigma}(\omega)=\frac{1}{i\hbar\omega}[R(\omega)-R(0)]\ . \tag{10b}$$

$R(\omega)$ is obtained by analytic continuation using N-point Padé approximants[13] from $R(i\nu_n)$, which is given, ignoring vertex corrections, by

$$R(i\nu_n)=-\frac{2k_BT}{N_{\mathbf{p}}^2}\sum_{\mathbf{p}\omega_n}\left[\frac{\partial\epsilon_{\mathbf{p}}}{\partial p_x a}\right]^2 \times G(\mathbf{p},i\omega_n)G(\mathbf{p},i\omega_n+i\nu_n)\ , \tag{10c}$$

where $N_{\mathbf{p}}^2$ is the total number of points in the Brillouin zone and $G(\mathbf{p},i\omega_n)$ is the no lines crossing Green's function obtained from Eqs. (4) and (5). The calculation is most effectively done in imaginary time; one uses a one-dimensional FFT to go from Matsubara space to imaginary time and vice-versa. The same Matsubara cutoff ($\sim$ three times the bandwidth) as in the Eliashberg equations was used in the calculation of the conductivity. In spite of this, finite-size effects are still present for small ν_n. For these, since $G(\mathbf{p},i\omega_n)\propto 1/\omega_n$ for large ω_n, the product of Green's functions in Eq. (10c) scales as $1/\omega_n^2$ as $\omega_n\to\infty$ and thus the sum over the Matsubara frequency ω_n is expected to deviate from its value for an infinite Matsubara cutoff by a term proportional to the inverse of the total number of Matsubara frequencies. This has been explicitly checked to be correct and the finite-size scaling analysis reveals that the finite Matsubara cutoff of ~ 6 eV turns out to affect the optical conductivity only for frequencies smaller than 10 meV, with the maximum effect at $\omega=0$ being of the order of 5%. Since impurities, which we have not taken into account, are also expected to affect the frequency dependence of the conductivity in this range of values of ω, we have ignored this fairly small effect in the results presented below.

Since we have shown that approximations borrowed from the electron-phonon problem fail to give a quantitative estimate of the critical temperature T_c, we would expect these approximations, as were used in Ref. (8), to be unreliable in the calculation of transport properties as well. This appears to be the case. We wish to stress the importance, when studying the normal-state properties of a strongly coupled system whose Fermi surface is relatively near a Van Hove singularity (as is the one studied in this paper), of calculating self-energy effects self-consistently, while taking into account the structure (in momentum and frequency space) of the effective interaction.

The temperature dependence of the resistivity $\rho=1/\mathrm{Re}\sigma(0)$ is shown in Fig. 7 for $t'=0$ and $t'=-0.45t$. In each case the coupling constant was chosen to give a transition temperature of 90 K and the chemical potential adjusted to obtain an electron density of $n=0.75$. We thus have no free parameters (apart for t') in our calculation of the normal-state charge response. ρ is obtained from the extrapolated value of $\mathrm{Re}\sigma(\omega)|_{\omega\to 0}$, since $\mathrm{Re}\sigma(\omega)\propto \mathrm{Im}R(\omega)/\omega$ and both quantities tend to zero as ω goes to zero. The small scatter in the data points reflects the difficulty in extrapolating to zero frequency from the analytic continuation. We have not calculated the resistivity for $T>250$ K, since we do not have the NMR data to determine the spin-fluctuation spectrum at these temperatures.

Our results show that not only are we able to obtain a resistivity that is linear in temperature from T_c up to 250 K, but that the magnitude of the resistivity at 90 K is in quantitative agreement with the best experimental values[17] [$28\ \mu\Omega\,\mathrm{cm}\le\rho(T_c)\le 55\ \mu\Omega\,\mathrm{cm}$, depending on the single crystal and the orientation of the applied field]. Our model does not take into account the orthorhombic

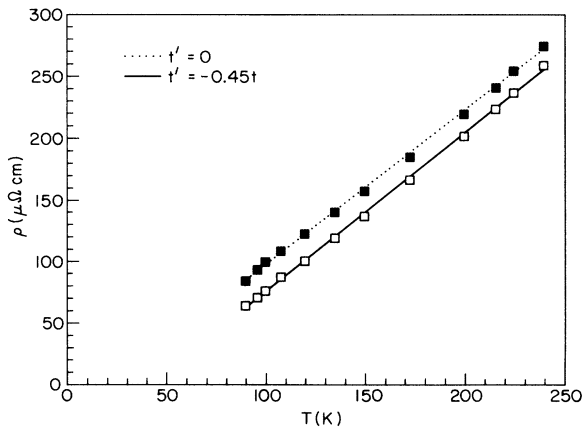

FIG. 7. The calculated resistivity due to spin-fluctuation scattering as a function of temperature for two choices of quasiparticle spectra, $t'=0$ (full squares and dotted line) and $t'=-0.45t$ (open squares and full line). For each of these choices the coupling constant g is taken to be that which yields $T_c=90$ K. The squares (open and full) are the calculated values, while the lines (dotted and full) are fits $\rho(T)=A+BT$. One obtains $A=-28.09\ \mu\Omega\,\mathrm{cm}$, $B=1.25\ \mu\Omega\,\mathrm{cm\,K^{-1}}$ for $t'=0$ and $A=-53.94\ \mu\Omega\,\mathrm{cm}$, $B=1.29\ \mu\Omega\,\mathrm{cm\,K^{-1}}$ for $t'=-0.45t$. The slope of 1.2–$1.3\ \mu\Omega\,\mathrm{cm\,K^{-1}}$ compares well with experiment. However, the intercepts are somewhat too negative.

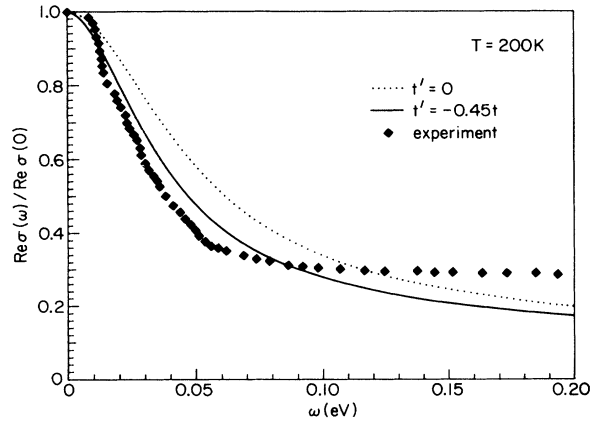

FIG. 8. The frequency dependence of the calculated optical conductivity (normalized to its value at $\omega=0$) at $T=200$ K for $t'=0$ (dotted line) and $t'=-0.45t$ (full line). For each of these choices the coupling constant g is taken to be that which yields $T_c=90$ K. The experimental points from Ref. 18 are denoted by diamonds.

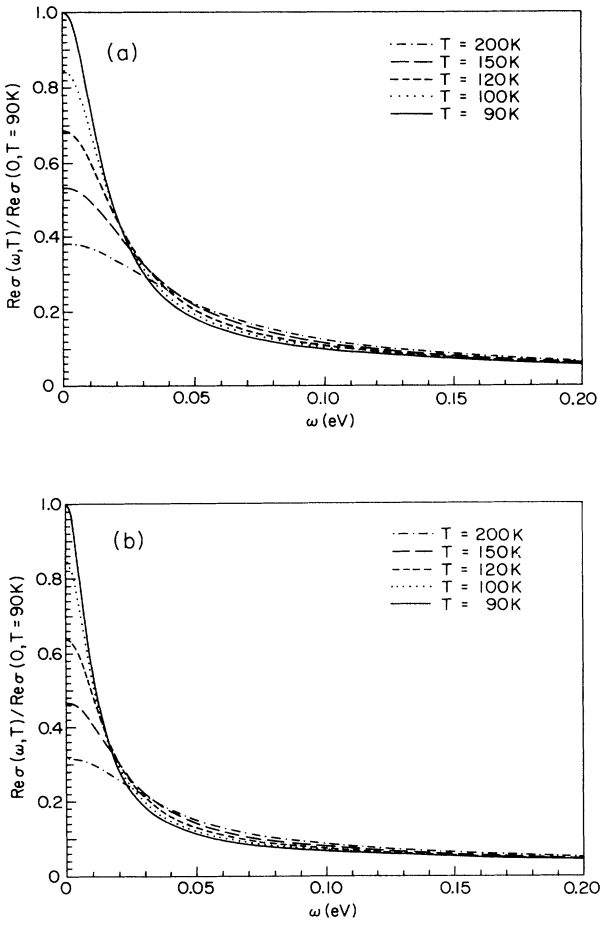

FIG. 9. The temperature and frequency of the conductivity (normalized to its value at $\omega=0$ and $T=90$ K). The parameters are the same as those specified in the caption to Fig. 8, for $t'=0$ (a) and $t'=-0.45t$ (b).

distortion in the a-b plane and the possibility of a different band mass in the a and b direction [i.e., $\partial\epsilon_{\mathbf{p}}/\partial p_x \neq \partial\epsilon_{\mathbf{p}}/\partial p_y$ in Eq. (10c)], which may be at the origin of this anisotropy. Note also that the smaller coupling constant in the case $t'=-0.45t$ results in a smaller resistivity at 90 K and that the slope of ρ versus T is nearly the same in both cases.

The frequency dependence of the conductivity at $T=200$ K is shown in Fig. 8 for $t'=0$ and $t'=-0.45t$ (in both cases the coupling constant is that required to obtain $T_c=90$ K) and compared to the experimental results of Orenstein *et al.*[18] When compared to the results of Arfi,[19] our results show that the frequency dependence of the conductivity is markedly influenced by quasiparticle lifetime effects. The improved quantitative agreement we obtain with the next-nearest-neighbor hopping, $t'=-0.45t$, provides another argument in favor of this assignment. In Figs. 9(a) and 9(b) we show the temperature dependence of the optical conductivity for frequencies up to 0.2 eV, for $t'=0$ [Fig. 9(a)] and $t'=-0.45t$ [Fig. 9(b)]. We postpone to a future paper a detailed comparison of these results with experiment.

V. SPIN EXCITATION SPECTRUM

We next examine the extent to which our model Hamiltonian provides a self-consistent description of the normal-state spin properties of $YBa_2Cu_3O_7$. To do so we first use our calculated quasiparticle excitation spectrum to determine the irreducible particle-hole spin susceptibility, $\tilde{\chi}(\mathbf{q},\omega)$, in the no lines crossing approximation; we then consider whether, with a momentum-dependent coupling, $J(\mathbf{q})$, between the irreducible particle-hole bubbles, $\tilde{\chi}(\mathbf{q},\omega)$, we can come close to retrieving our input spin susceptibility, $\chi_{\mathrm{MMP}}(\mathbf{q},\omega)$.

In the Matsubara frequency representation $\tilde{\chi}(\mathbf{q},\omega)$ is given by

$$\tilde{\chi}(\mathbf{q},i\nu_n)=-\frac{2k_BT}{N_{\mathbf{p}}^2}\sum_{\mathbf{p},\omega_n} G(\mathbf{p},i\omega_n)G(\mathbf{p}+\mathbf{q},i\omega_n+i\nu_n)\ , \quad (11)$$

where $N_{\mathbf{p}}^2$ is the number of points in the Brillouin zone. $\tilde{\chi}(\mathbf{q},i\nu_n)$ is seen to be the autocorrelation of the single-particle Green's function. Autocorrelations, as for convolutions (i.e., one-loop Eliashberg equations), are most efficiently performed using a FFT algorithm. To be consistent, the number of points in the Brillouin zone and the Matsubara cutoff were chosen to be the same as those used in the solution of the Eliashberg equations. As was mentioned in connection with the optical conductivity, the finite Matsubara cutoff produces finite-size effects of the order of the inverse of the total number of Matsubara frequencies. We have not carried out a finite-size scaling analysis in this case, but the error should be of the same order of magnitude as in the case of the conductivity and it should not affect our main conclusions.

The static irreducible susceptibility $\tilde{\chi}(\mathbf{q},0)$ is shown in Figs. 10(a) and 10(b) for $t'=0$ and $t'=-0.45t$. Also shown is the susceptibility $\tilde{\chi}_0(\mathbf{q},0)$ one obtains with bare Green's functions in Eq. (11). The considerable structure present in $\tilde{\chi}_0(\mathbf{q},0)$, which reflects the Kohn anomalies as-

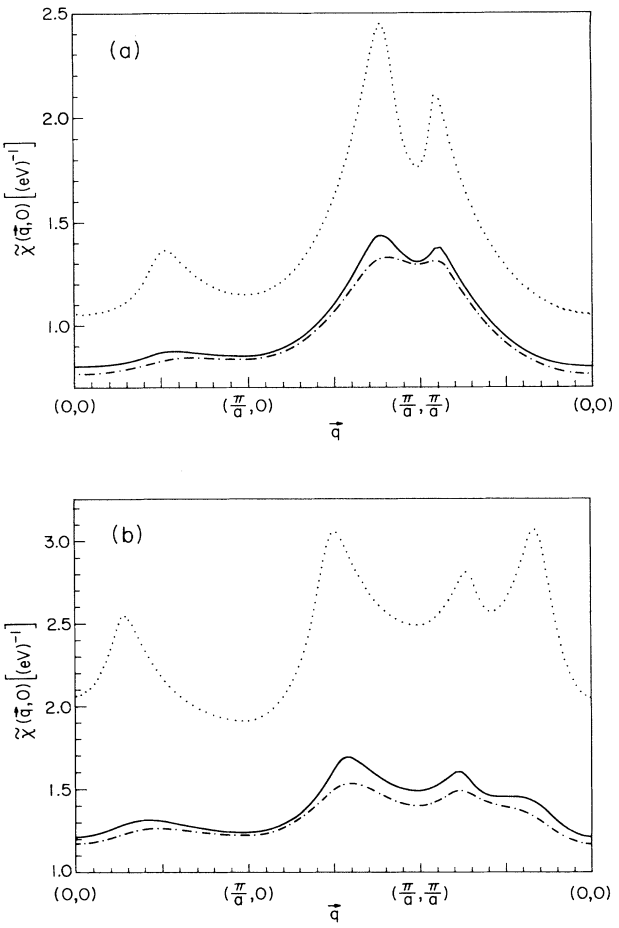

FIG. 10. The irreducible particle-hole susceptibility $\tilde{\chi}(\mathbf{q},0)$ calculated using bare propagators (dotted line) and in the no lines crossing approximation at $T=90$ K (full line) and $T=200$ K (dash-dotted line) for $t'=0$ (a) and $t'=-0.45t$ (b).

sociated with transitions that span the Fermi surface, is considerably modified by lifetime effects, while the magnitude of the susceptibility is reduced. One also notices that the Kohn anomaly peaks are further away from the commensurate wave vector $(\pi/a,\pi/a)$ when using the quasiparticle spectrum with next-nearest-neighbor hopping $t'=-0.45t$. The change in temperature of $\tilde{\chi}(\mathbf{q},0)$ seen in Figs. 10(a) and 10(b) likewise reflects the consequence of quasiparticle scattering against spin fluctuations, since at higher temperatures the quasiparticle lifetime is shorter. The calculated percentage reduction with increasing temperature is nearly twice as large in the vicinity of $(\pi/a,\pi/a)$ as near $\mathbf{q}=0$; in other words, the commensurate irreducible spin susceptibility is more susceptible to lifetime effects than is the long-wavelength $\tilde{\chi}(\mathbf{q},0)$.

We have also calculated the low-frequency quasiparticle response $\mathrm{Im}\tilde{\chi}(\mathbf{q},\omega)/\omega$, which is of importance for NMR experiments, for $t'=-0.45t$, using N-point Padé approximants.[13] As may be seen in Fig. 11, apart from the expected peak near $\mathbf{q}=0$ [in the absence of lifetime effects $\mathrm{Im}\tilde{\chi}(\mathbf{q},\omega)$ would vary as q^{-1} in the collisionless

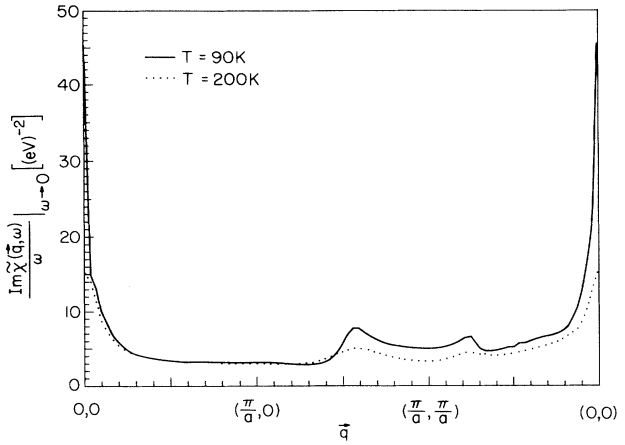

FIG. 11. The low-frequency irreducible dynamic particle-hole susceptibility $\mathrm{Im}\tilde{\chi}(\mathbf{q},\omega)/\omega$, as a function of $\mathbf{q}$ at $T=90$ K (full line) and $T=200$ K (dotted line).

limit of interest to us here], $\mathrm{Im}\tilde{\chi}(\mathbf{q},\omega)/\omega$ is remarkably featureless [the two small peaks near $(\pi/a,\pi/2a)$ and $(3\pi/4a,3\pi/4a)$ reflect the Kohn anomalies]. The quasiparticle spectrum with a $t'\neq 0$ is very important in calculating $\mathrm{Im}\tilde{\chi}(\mathbf{q},\omega)/\omega$ at low frequencies; it enables one to get a nonzero answer at $\mathbf{q}=\mathbf{Q}$, since with this spectrum $\mathbf{Q}$ is a wave vector that spans the Fermi surface. With the nearest-neighbor tight-binding spectrum ($t'=0$), all the wave vectors spanning the Fermi surface are smaller in magnitude than $\mathbf{Q}$, as we pointed out earlier. Thus, one should have $\mathrm{Im}\tilde{\chi}(\mathbf{Q},\omega)=0$, as $\omega\rightarrow 0$, and therefore a much weaker NMR response. Another quantity of interest is the characteristic energy, $\tilde{\Gamma}(\mathbf{q})$, defined, for $\omega\rightarrow 0$, by

$$\mathrm{Im}\tilde{\chi}(\mathbf{q},\omega)=\pi\tilde{\chi}(\mathbf{q},0)\omega/\tilde{\Gamma}(\mathbf{q})\ , \tag{12}$$

which measures the low-frequency quasiparticle magnetic response. Figure 12 shows $\tilde{\Gamma}(\mathbf{q})$ for $T=90$ K and

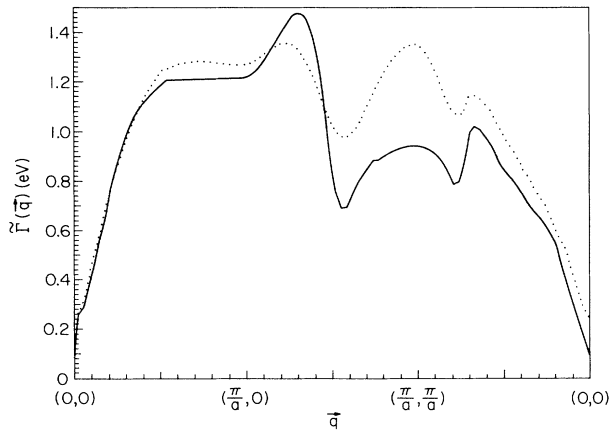

FIG. 12. The characteristic energy $\tilde{\Gamma}(\mathbf{q})$, which measures the low-frequency "irreducible" quasiparticle response [see Eq. (12)] as a function of $\mathbf{q}$ for $T=90$ K (full line) and $T=200$ K (dotted line).

$T=200$ K. The temperature dependence and structure for wave vectors near $(\pi/a,\pi/a)$ reflects the interplay between the momentum and temperature dependence of $\tilde{\chi}(\mathbf{q},0)$ [Fig. 10(b)] and that of $\mathrm{Im}\tilde{\chi}(\mathbf{q},\omega)/\omega$ (Fig. 11).

Both the reduction of the incommensurate Kohn anomaly peaks of $\tilde{\chi}(\mathbf{q},0)$ and their relative distance from $(\pi/a,\pi/a)$ seen in Fig. 10(b) are also essential features; as shown below they allow us, to the extent that vertex corrections may be neglected, to obtain a commensurate random-phase approximation (RPA) susceptibility

$$\chi(\mathbf{q},\omega)=\frac{\tilde{\chi}(\mathbf{q},\omega)}{1-J(\mathbf{q})\tilde{\chi}(\mathbf{q},\omega)} , \tag{13}$$

with a momentum-dependent coupling $J(\mathbf{q})$ between the particle-hole "bubbles" $\tilde{\chi}(\mathbf{q},\omega)$, which is peaked at $(\pi/a,\pi/a)$ and has a range of the order of one lattice spacing. It is natural to enquire whether there exists a $J(\mathbf{q})$, which for low frequencies, brings $\chi(\mathbf{q},\omega)$ close to the input susceptibility $\chi_{\mathrm{MMP}}(\mathbf{q},\omega)$, the MMP low-frequency response function which provides a quantitative account of NMR experiments. To facilitate the comparison, note that for low frequencies $\mathrm{Im}\tilde{\chi}(\mathbf{q},\omega)$ is given by Eq. (12) and that $\mathrm{Re}\tilde{\chi}(\mathbf{q},\omega)\simeq\tilde{\chi}(\mathbf{q},0)$. Then the imaginary part of Eq. (13) at low frequency reduces to

$$\mathrm{Im}\chi(\mathbf{q},\omega)=\frac{\tilde{\chi}(\mathbf{q},0)\pi\omega/\Gamma(\mathbf{q})}{[1+F^a(\mathbf{q})]^2+[F^a(\mathbf{q})\pi\omega/\Gamma(\mathbf{q})]^2} , \tag{14}$$

where

$$F^a(\mathbf{q})=-J(\mathbf{q})\tilde{\chi}(\mathbf{q},0) \tag{15}$$

measures the strength of the momentum-dependent "Fermi-liquid" correction to the irreducible susceptibility $\tilde{\chi}(\mathbf{q},\omega)$,

$$\chi(\mathbf{q},0)=\frac{\tilde{\chi}(\mathbf{q},0)}{1+F^a(\mathbf{q})} . \tag{16}$$

Expressing $\tilde{\chi}(\mathbf{q},0)$ in terms of $\chi(\mathbf{q},0)$ from Eq. (16), Eq. (14) may be written, after a trivial rearrangement, as

$$\mathrm{Im}\chi(\mathbf{q},\omega)=\frac{\chi(\mathbf{q},0)\omega/\omega_{\mathrm{SF}}(\mathbf{q})}{1+[F^a(\mathbf{q})\omega/\omega_{\mathrm{SF}}(\mathbf{q})]^2} , \tag{17}$$

where

$$\omega_{\mathrm{SF}}(\mathbf{q})=\frac{\tilde{\Gamma}(\mathbf{q})[1+F^a(\mathbf{q})]}{\pi} . \tag{18}$$

A comparison of Eq. (14) with Eq. (2) shows that in the vicinity of the commensurate antiferromagnetic wave vector $(\pi/a,\pi/a)$, where $F^a(\mathbf{q})\sim-1$, $\mathrm{Im}\chi(\mathbf{q},\omega)$ is of the MMP form, Eq. (2).

In choosing a $J(\mathbf{q})$, or what is equivalent, $F^a(\mathbf{q})$, which yields an expression close to the phenomenological expression used by MMP, we were guided by the two limiting values,

$$F^a(\mathbf{q}=0)=-0.535 , \tag{19a}$$

$$F^a(\mathbf{q}=\mathbf{Q})=-0.965 , \tag{19b}$$

which are required to yield the long-wavelength susceptibility, $\chi_0=2.62$ states/eV, and the commensurate susceptibility, $\chi_{\mathbf{Q}}=44$ states/eV found in the MMP analyses. To obtain a RPA susceptibility, Eq. (13), which is peaked at the commensurate wave vector $(\pi/a,\pi/a)$, most of the dispersion in $J(\mathbf{q})$ has to occur between the Kohn anomalies of $\tilde{\chi}(\mathbf{q},0)$ shown in Fig. 10(b). A functional form of $J(\mathbf{q})$ that achieves this is

$$J(\mathbf{q})=J_0+\frac{J_1}{1+2\xi_J^2[2+\cos(q_x a)+\cos(q_y a)]} , \tag{20}$$

which is peaked at $\tilde{Q}$, with the dispersion of that peak determined by ξ_J^2. We determined ξ_J^2 by taking the dispersion of $\tilde{\chi}(\mathbf{q},0)$ in the vicinity of $\mathbf{Q}=(\pi/a,\pi/a)$ into account and requiring that the dispersion of $\chi(\mathbf{q},0)$ around $\mathbf{Q}$ be of the MMP form. At $T=90$ K, the values $J_0=0.399$ eV, $J_1=0.250$ eV, and $\xi_J^2=0.761$ were found to give a $\chi(\mathbf{q},0)$ in good agreement with the MMP form. Our calculated value of $F^a(\mathbf{q})$ is shown in Fig. 13. $\chi(\mathbf{q},0)$ is compared to the MMP results at $T=90$ K in Fig. 14, while our calculated $\mathrm{Im}\chi(\mathbf{q},\omega)/\omega$ evaluated in the low-frequency limit is compared with the MMP result in Fig. 15. The maximum of $\mathrm{Im}\chi_{\mathrm{MMP}}(\mathbf{q},\omega)/\omega$, at $\mathbf{q}=(\pi/a,\pi/a)$, is $\chi(\mathbf{q},0)/\omega_{\mathrm{SF}}$. The slight discrepancy between our calculated $\mathrm{Im}\chi(\mathbf{q},\omega)/\omega$ and MMP near $\mathbf{Q}$ is due to the fact that the calculated ω_{SF} from Eq. (18) is about 10 meV, to be compared with the value found by MMP, 8 meV.

Figure 16 shows the dynamic structure factor

$$S(\mathbf{q},\omega)=\left[\frac{1}{1-\exp\left[-\frac{\omega}{k_B T}\right]}\right]\mathrm{Im}\chi(\mathbf{q},\omega)$$

as a function of momentum for $\omega=3$, 6, 12, and 15 meV at $T=90$ K with the same $J(\mathbf{q})$. It will be interesting to compare this calculation with the results of neutron-scattering experiments once a consensus has been reached on $YBa_2Cu_3O_7$.

If we assume that J_0, J_1, and ξ_J^2 do not depend on temperature, a comparison of our calculated values of $\chi(\mathbf{q},0)$ and $\mathrm{Im}\chi(\mathbf{q},\omega)/\omega$ at $T=200$ K with the MMP values

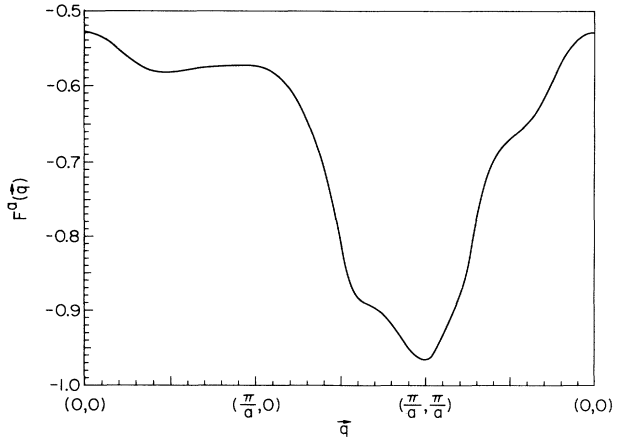

FIG. 13. The value of $F^a(\mathbf{q})$ at $T=90$ K, calculated using the $J(\mathbf{q})$ parameters cited in the text, and the calculated value of $\tilde{\chi}(\mathbf{q},0)$.

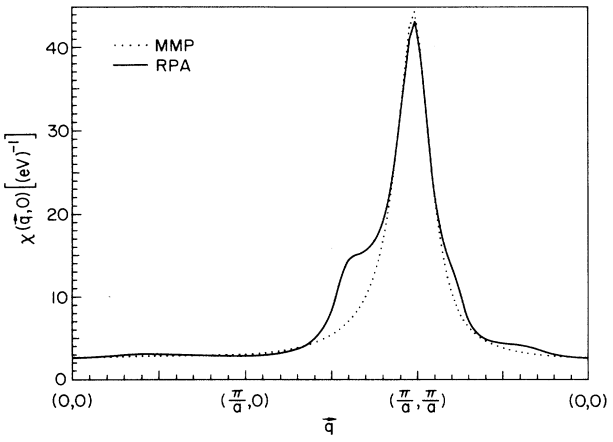

FIG. 14. The calculated value of $\chi(\mathbf{q},0)$ at $T=90$ K (full line) compared with the MMP result (dotted line). The shoulders in the calculated value reflect the influence of Kohn anomalies in $\tilde{\chi}(\mathbf{q},0)$ depicted in Fig. 10(b).

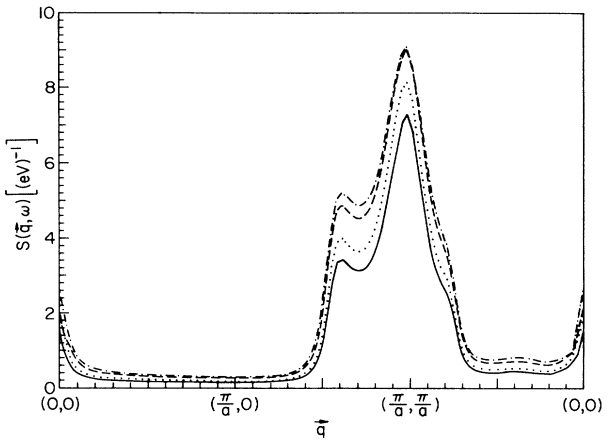

FIG. 16. The calculated dynamic structure factor $S(\mathbf{q},\omega)=\{1/[1-\exp(-\omega/k_BT)]\}\mathrm{Im}\chi(\mathbf{q},\omega)$ at $T=90$ K as a function of $\mathbf{q}$ for $\omega=3$ meV (full line), $\omega=6$ meV (dotted line), $\omega=12$ meV (dashed line), and $\omega=15$ meV (dash-dotted line).

shows significant discrepancies. On the other hand, it is straightforward to get a good fit by assuming a temperature-dependent $J(\mathbf{q},T)$, as done for example by Moriya, Takahashi, and Ueda, in their self-consistent renormalization approach.[20]

The rather good agreement between $\chi(\mathbf{q},\omega)$ and the phenomenological expression $\chi_{\mathrm{MMP}}(\mathbf{q},\omega)$ is encouraging; it offers hope that a self-consistent expression for $\chi(\mathbf{q},\omega)$ that provides a good quantitative account of NMR experiments can be obtained, in the sense that the spectral density used in the calculation of the quasiparticle excitation spectrum, and hence of $\tilde{\chi}(\mathbf{q},\omega)$, will, for a suitable choice of $J(\mathbf{q})$, yield that same response function on making use of Eq. (13). Indeed, since $\chi(\mathbf{q},\omega)$ is close to the input $\chi_{\mathrm{MMP}}(\mathbf{q},\omega)$, it may turn out that with values of $J(\mathbf{q})$ not far from those considered above, one can achieve self-consistency. We are currently examining this possibility.

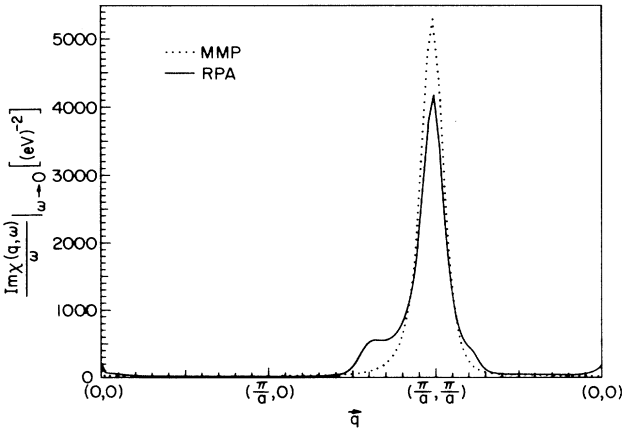

FIG. 15. The calculated value of $\mathrm{Im}\chi(\mathbf{q},\omega)/\omega$ at $T=90$ K (full line) compared with the MMP result (dotted line). The shoulders in the calculated value reflect the influence of Kohn anomalies on both $\tilde{\chi}(q,0)$, depicted in Fig. 10(b), and on $\mathrm{Im}\tilde{\chi}(\mathbf{q},\omega)$, depicted in Fig. 11.

VI. CONCLUSION

In this paper we report on strong-coupling calculations, which demonstrate that antiferromagnetic spin fluctuations can yield high-temperature superconductivity in a 2D system in which the parameters that specify both the quasiparticle and spin excitations are chosen from experiments on $YBa_2Cu_3O_7$. The anomalous optical and transport properties of this system have been calculated and found to agree with some key aspects of experiment. The results provide strong support for the proposal that the planar quasiparticle excitations in $YBa_2Cu_3O_7$ form a nearly antiferromagnetic Fermi liquid, which exhibits a transition at ~ 90 K to a superconducting $d_{x^2-y^2}$ pairing state of purely electronic origin.

As in a normal Fermi liquid, the spin and charge properties of the nearly antiferromagnetic Fermi liquid, which describes $YBa_2Cu_3O_7$ are not separated; both are determined by quasiparticle interactions. The anomalous properties of the system come about because of the coupling of quasiparticles to low-frequency spin fluctuations whose spectrum is sharply peaked at the commensurate wave vector $(\pi/a,\pi/a)$. The sharp features that characterize the tunneling density of states, the weak-coupling gap, the first-order quasiparticle self-energy, and the quasiparticle response are smoothed out. The wave function renormalization constant Z_p is found to vary between 0.4 and 0.6 as one goes around the Fermi surface. Despite the fact that for a wide range of temperatures and energies, the imaginary part of the self-energy varies as ω or as T, rather than the ω^2 or T^2 variation familiar from ordinary Fermi liquids, the nearly antiferromagnetic Fermi liquid *is* a Fermi liquid; were it not for the superconducting transition at low enough temperatures one would find $\mathrm{Im}\Sigma(\mathbf{p},\omega,T)\sim\omega^2\ln(\omega)$ or $T^2\ln(T)$ (depending

on whether one takes the $T \to 0$ or $\omega \to 0$ limit) characteristic of normal 2D Fermi liquids, while explicit calculation shows that Luttinger's theorem is obeyed.

While our numerical calculations provide the necessary "proof of concept" for spin-fluctuation superconductivity and lead to an appealing description of the normal-state properties of $YBa_2Cu_3O_7$, a number of challenging theoretical problems remain, of which we mention three here: (i) Can an effective spin coupling $J(\mathbf{q})$, be found that yields a self-consistent description of the normal state which agrees with experiment for $YBa_2Cu_3O_7$? (ii) Can one extend this approach to the entire YBaCuO family, where, as a result of lower oxygen content (and reduced hole doping) the spin susceptibility becomes temperature dependent, and T_c is lowered? (iii) Can the dependence of coupling on hole concentration be derived microscopically?

In conclusion, we wish to emphasize that the correctness of the nearly antiferromagnetic Fermi-liquid approach we have described will not be determined theoretically, but by experiment. If the pairing state of $YBa_2Cu_3O_7$ is proved to be other than the $d_{x^2-y^2}$ state unambiguously predicted by our theory, then our theory, no matter how appealing it might be, and no matter how well it describes the normal state, does not apply to $YBa_2Cu_3O_7$. A direct test of the pairing state is thus highly desirable, as are the theoretical calculations of the superconducting properties, which will make possible a quantitative comparison of theory with experiment.

ACKNOWLEDGMENTS

We should like to thank E. Abrahams, J. Annett, B. Arfi, A. Balatsky, N. E. Bickers, N. Goldenfeld, L. P. Gor'kov, A. Kampf, J.-P. Lu, A. J. Millis, T. M. Rice, D. J. Scalapino, H. Schultz, J. R. Schrieffer, and D. Thelen for stimulating discussions on these and related topics, and the Aspen Center for Physics and the Los Alamos National Laboratory for their hospitality to one of us (D.P.) during the preparation of the manuscript. The research described in this paper has been supported by NSF Grant No. DMR88-17613, in part, by the National Science Foundation (Grant No. DMR88-09854) through the Science and Technology Center for Superconductivity, and, in part, by the program on strongly correlated electron systems of the Los Alamos National Laboratory. The calculations were performed on the Cray Y-MP at the National Center for Supercomputing Applications at the University of Illinois at Urbana-Champaign, and we thank R. Nandkumar and L. Smarr for their support and encouragement.

[1] J. G. Bednorz and K. A. Mueller, Z. Phys. B **64**, 189 (1986).

[2] N. E. Bickers, D. J. Scalapino, and R. T. Scalettar, Int. J. Mod. Phys. B **1**, 687 (1987); N. E. Bickers, D. J. Scalapino, and S. R. White, Phys. Rev. Lett. **62**, 961 (1989); N. E. Bickers and S. R. White, Phys. Rev. B **43**, 8044 (1991).

[3] P. Monthoux, A. V. Balatsky, and D. Pines, Phys. Rev. Lett. **67**, 3448 (1991).

[4] P. Monthoux, A. V. Balatsky, and D. Pines, Phys. Rev. B **46**, 14803 (1992).

[5] P. Monthoux and D. Pines, Phys. Rev. Lett. **69**, 961 (1992).

[6] K. Ueda, T. Moriya, and Y. Takahashi, *Electronic Properties and Mechanisms of High-T_c Superconductors,* edited by Oguchi *et al.* (North-Holland, Amsterdam, 1992), p. 145; (unpublished).

[7] A. J. Millis, S. Sachdev, and C. M. Varma, Phys. Rev. B **37**, 4975 (1989).

[8] R. J. Radtke, S. Ullah, K. Levin, and M. R. Norman, Phys. Rev. B **46**, 11 975 (1992).

[9] A. J. Millis, H. Monien, and D. Pines, Phys. Rev. B **42**, 167 (1990).

[10] J. C. Campuzano, G. Jennings, M. Faiz, L. Beaulaigue, B. W. Veal, J. Z. Liu, A. P. Paulikas, K. Vandervoort, H. Claus, R. S. List, A. J. Arko, and R. J. Bartlett, Phys. Rev. Lett. **64**, 2308 (1990).

[11] G. M. Eliashberg, Zh. Eksp. Teor. Fiz. **38**, 966 (1960) [Sov. Phys. JETP **11**, 696 (1960)].

[12] A. J. Millis, Phys. Rev. B **45**, 13 047 (1992).

[13] H. J. Vidberg and J. W. Serene, J. Low Temp. Phys. **29**, 177 (1977).

[14] A. P. Kampf and J. R. Schrieffer, Phys. Rev. B **41**, 6399 (1990); **42**, 7967 (1990).

[15] J. E. Hirsch and D. J. Scalapino, Phys. Rev. Lett. **56**, 2732 (1986).

[16] P. Monthoux (unpublished).

[17] J. P. Rice, J. Giapintzakis, D. M. Ginsberg, and J. M. Mochel, Phys. Rev. B **44**, 10 158 (1991).

[18] J. Orenstein, G. A. Thomas, A. J. Millis, S. L. Cooper, D. H. Rapkine, T. Timusk, L. F. Schneemeyer, and J. V. Waszczak, Phys. Rev. B **42**, 6342 (1990).

[19] B. Arfi, Phys. Rev. B **45**, 2352 (1992).

[20] T. Moriya, Y. Takahashi, and K. Ueda, J. Phys. Soc. Jpn. **52**, 2905 (1990); Physica C **185-189**, 114 (1990).